

Field-Effect Transistor Based on MoSi_2N_4 and WSi_2N_4 Monolayers Under Biaxial Strain: A Computational Study of the Electronic Properties

Nayereh Ghobadi, Manouchehr Hosseini, and Shoeib Babaei Touski

Abstract—The electronic properties of a field-effect transistor with two different structures of MoSi_2N_4 and WSi_2N_4 monolayers as the channel material in the presence of biaxial strain are investigated. The band structures show that these compounds are semiconductors with an indirect bandgap. Their band gaps can be adjusted by applying in-plane biaxial strain. In the following, the variation of the energies of the valleys and corresponding effective masses with respect to the strain are explored. Finally, the strained MoSi_2N_4 or WSi_2N_4 are used as the channel of a p-type FET and the corresponding current-voltage characteristic is explored. The results show this FET has an $I_{\text{ON}}/I_{\text{OFF}}$ ratio larger than 10^6 and subthreshold swing in the range of 96-98 mV/dec. The $I_{\text{ON}}/I_{\text{OFF}}$ ratio of these compounds with respect to strain are compared.

Index Terms— MoSi_2N_4 , WSi_2N_4 , Biaxial Strain, Field-Effect Transistor, $I_{\text{ON}}/I_{\text{OFF}}$ ratio, Sub-threshold swing.

I. INTRODUCTION

TWO-dimensional materials are being widely studied from 2004 with the successful experimental isolation of graphene [1]. Graphene with full-sp² carbon atoms exhibits the remarkable electronic properties [2]–[4], however, absence of an energy gap seriously precluded its exploitation in electronic applications [5], [6]. Efforts to create an energy gap in graphene were ineffective [5], [7], [8], and researches extend into other two-dimensional materials such as the transition metal dichalcogenides (TMDs) [9]–[11], indium selenide [12], indium telluride [13], and phosphorene [14] with appropriate energy gaps. The design of new 2D materials with attractive piezoelectricity and flexoelectricity is very attractive to expand the practical application of two-dimensional materials [15], [16].

Single-layer MA_2Z_4 (M = early transition metal, e.g. Mo, W, and Nb; A = Si or Ge, Z = N, P or As), is a family of materials with covering semiconducting, metallic and magnetic properties [17]–[19]. A single layer MoA_2Z_4 is composed of an M-A sub-layer sandwiched between two A-Z sub-layers. Researchers are predicted high lattice thermal conductivity of 440 and 500 W/mK [20], and elastic modulus of 487 and 506 GPa for a single layer of MoSi_2N_4 and WSi_2N_4 which have made them attractive 2D materials. Synthesizing with a large size of 2D MoSi_2N_4 [21], the excellent ambient stability of it [21], [22], besides the large theoretical electron/hole mobilities

N. Ghobadi is with the Department of Electrical Engineering, University of Zanjan, Zanjan, Iran. M. Hosseini is with the Department of Electrical Engineering, Bu-Ali Sina University, Hamedan, Iran e-mail:(m.hosseini@basu.ac.ir). S. B. Touski is with the Department of Electrical Engineering, Hamedan University of Technology, Hamedan, Iran.

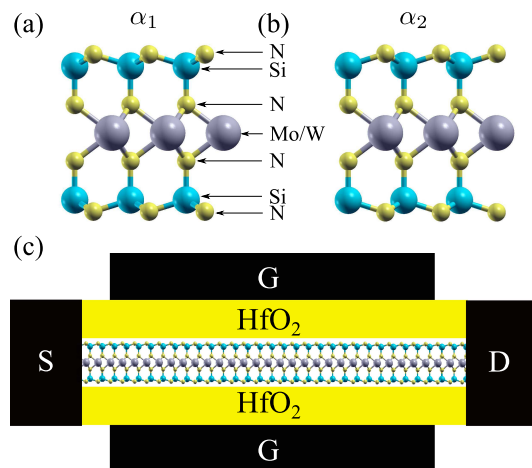


Fig. 1. Schematic of MoSi_2N_4 and WSi_2N_4 with (a) α_1 - and (b) α_2 -configurations. (c) The configuration of the studied DGFET with MoSi_2N_4 and WSi_2N_4 as the channel.

(up to $270/1200 \text{ cm}^2/(\text{Vs})$) which are near to six times larger than those of monolayer MoS_2) creates a bright and versatile future for this material [21], [22]. MoSi_2N_4 and WSi_2N_4 have an indirect bandgap with the values of 1.73 eV and 2.06 eV, respectively [17], [23]. This range of bandgap makes them promising candidates for potential optical applications in the visible range. This family has a pair of valley pseudospins. Therefore, these materials have suitable valleytronic properties to be applied in multiple information processing in the future [24].

It is expected that MA_2Z_4 family demonstrate potential applications ranging from electronics, optoelectronics, photonics, spintronics, catalysis to energy harvesting [20]. With sandwiching a TMD-type MZ_2 monolayer into InSe-type A_2Z_2 in MA_2Z_4 monolayers, twelve different structures have been achieved [18]. It has been reported that α_1 and α_2 constructions of MoSi_2N_4 and WSi_2N_4 are the most stable structures [18]. It has been shown that this material can withstand strain values up to 19.5 percentage [25]. The effect of biaxial strain on the electronic properties of these stable constructions as the channel material of a FET has not been explored. Therefore, in this work, we have investigated the electronic properties of α_1 and α_2 constructions of MoSi_2N_4 and WSi_2N_4 in the presence of in-plane biaxial strain with first-principles calculations. In the following, we use a ballistic analytical model as the top-of-the-barrier model to assess

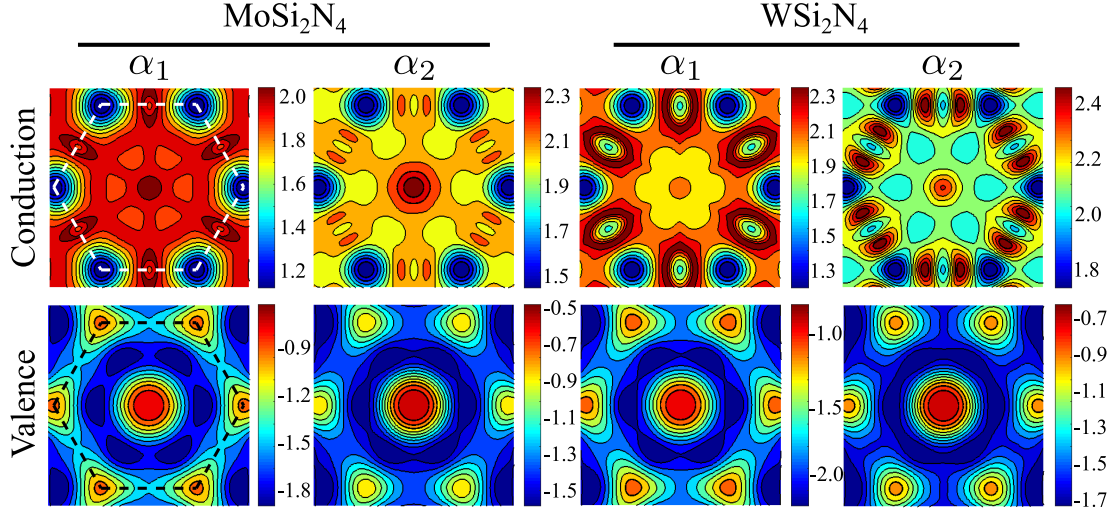


Fig. 2. The two-dimensional energy map of the conduction and valence bands for all compounds. The first Brillouin zone is indicated for both conduction and valence band of α_1 -MoSi₂N₄.

the DC performance of the double-gate field-effect transistor (DGFET) based on single-layer MoSi₂N₄ and WSi₂N₄ under biaxial strain [26], [27].

Some details on the ab initio calculations of the electronic properties in the presence of strain are discussed in Section II. In Section III, The effects of biaxial strain on the electronic properties have been explored and DC performance of the DGFETs based on these materials have been investigated in section IV. Finally, concluding remarks are presented in Section VI.

II. COMPUTATIONAL DETAILS

In order to investigate the properties of MoSi₂N₄ and WSi₂N₄ monolayers, density functional calculations are performed using the SIESTA software [28]. The generalized gradient approximation (GGA) with the Perdew-Burke-Ernzerhof (PBE) [29] functional is employed for the exchange-correlation term. A Monkhorst-Pack k-point grid of $21 \times 21 \times 1$ is chosen for the unit cell. A double- ζ plus polarization basis set is used and the energy cutoff is 200 Ry. The total energy is converged to better than 10^{-5} eV. The structures are fully relaxed until the force on each atom is less than 0.02 eV/Å. To avoid interactions in the normal direction, a vacuum region of 30 Å is added. To visualize the atomic structures, the XCrySDen package has been used [30]. The in-plane biaxial strain is defined as $\varepsilon = (a - a_0)/a_0$, where a_0 and a are the equilibrium and deformed lattice constants, respectively. The effective mass of the carriers is calculated using the following equation [31],

$$m^* = \hbar^2 / (\partial^2 E / \partial k^2) \quad (1)$$

Here, \hbar is the reduced Planck constant, E and k are the energy and wave vector of conduction band minimum and valence band maximum.

III. RESULTS AND DISCUSSION

Two different configurations of MoSi₂N₄ and WSi₂N₄ have been reported to have the lowest energy [18]. However, the

TABLE I
THE LATTICE CONSTANT (A), THE M-N (d_{M-N}) AND SI-N (d_{Si-N}) BOND LENGTHS, THE VERTICAL DISTANCE BETWEEN SI AND N ATOMS (Δ_{Si-N}), THE THICKNESS AND THE COHESIVE ENERGIES (E_{coh}) OF MoSi₂N₄ AND WSi₂N₄ MONOLAYERS.

	a (Å)	d_{M-N} (Å)	d_{Si-N} (Å)	Δ_{Si-N} (Å)	E_{coh} (eV/atom)
α_1 -MoSi ₂ N ₄	2.935	2.122	1.764	0.53	-8.855
α_2 -MoSi ₂ N ₄	2.926	2.122	1.774	0.545	-8.834
α_1 -WSi ₂ N ₄	2.949	2.137	1.761	0.519	-8.942
α_2 -WSi ₂ N ₄	2.939	2.141	1.773	0.537	-8.919

energy difference between these two structures is small. The schematic of MoSi₂N₄ and WSi₂N₄ with these two constructions, α_1 and α_2 , have been shown in Fig. 1. A MoN₂ sub-layer is sandwiched between two SiN sub-layers. In the α_2 -structure, these three sub-layers are exactly placed over others, whereas two SiN sub-layers have shift respect to MoN₂ sub-layer in α_1 -structure. The configuration of the studied FET is sketched in Fig. 1(c). A monolayer MoSi₂N₄ or WSi₂N₄ and a high-K thin-film HfO₂ have been used as the channel material and gate dielectric, respectively.

The structural properties of these four materials are reported in Table I. The lattice constants of these four materials are in the same range and are compatible with previously reported works [18], [21]. However, α_2 -structure demonstrates a slightly lower lattice constant than α_1 one. On the other hand, the cohesive energies are also in the same range, whereas α_1 demonstrates lower cohesive energy and is more stable. In addition, WSi₂N₄ has a lower cohesive energy than MoSi₂N₄. The thickness of these compounds is approximately the same and α_2 -configuration has a higher thickness. Finally, the buckling height of the SiN sub-layer demonstrates a higher value in α_2 -configuration.

Two-dimensional map of conduction and valence bands in the first Brillouin zone for all compounds is plotted in Fig. 2. It is obvious that the conduction band minimum (CBM) is located at K-valley for all these materials. However, WSi₂N₄

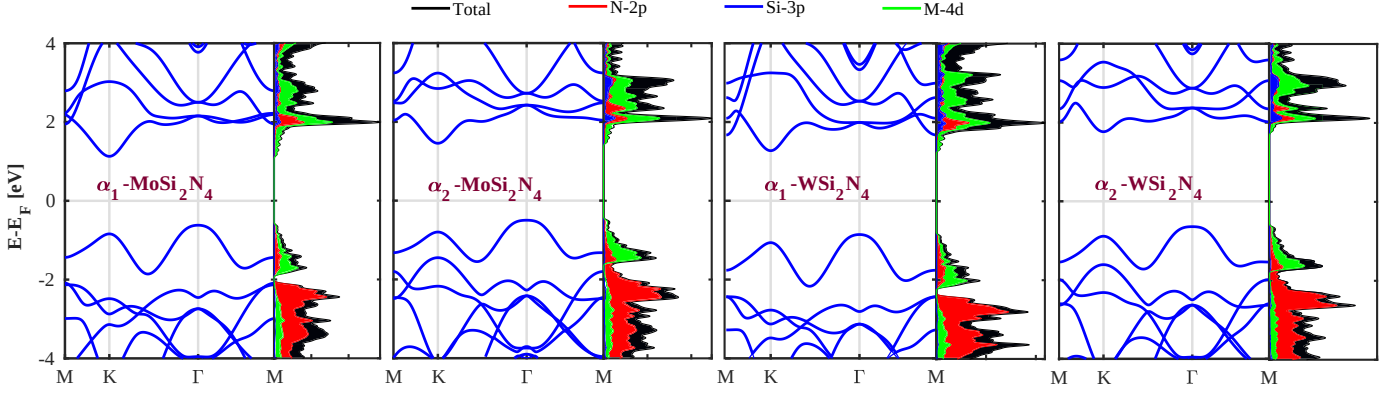


Fig. 3. The band structures of MoSi_2N_4 and WSi_2N_4 with α_1 - and α_2 -configuration. The projected density of states are plotted alongside of its corresponding band structure.

TABLE II

THE CALCULATED BAND GAPS (E_g), POSITION OF VBM AND CBM, THE ENERGIES OF CONDUCTION (E_C-E_F) AND VALENCE BAND (E_V-E_F) EDGES, AND THE EFFECTIVE MASSES AT K AND Γ -POINT OF THE VALENCE BAND AND K-VALLEY OF THE CONDUCTION BAND.

	E_g (eV)	VBM	CBM	E_C-E_F (eV)	E_V-E_F (eV)	$m_{K \rightarrow M}^{v,*}$ (m_0)	$m_{K \rightarrow \Gamma}^{v,*}$ (m_0)	$m_{\Gamma \rightarrow K}^{v,*}$ (m_0)	$m_{\Gamma \rightarrow M}^{v,*}$ (m_0)	$m_{K \rightarrow M}^{c,*}$ (m_0)	$m_{K \rightarrow \Gamma}^{c,*}$ (m_0)
α_1 - MoSi_2N_4	1.748	Γ	K	1.129	-0.619	0.838	0.621	1.319	1.314	0.626	0.551
α_2 - MoSi_2N_4	1.954	Γ	K	1.456	-0.497	0.944	0.814	1.589	1.61	0.639	0.628
α_1 - WSi_2N_4	2.129	Γ	K	1.272	-0.857	0.728	0.569	1.206	1.196	0.525	0.519
α_2 - WSi_2N_4	2.41	Γ	K	1.766	-0.644	0.797	0.727	1.52	1.545	0.578	0.753

displays a local minimum at M-valley with an energy close to K-valley. On the other hand, the valence band maximum (VBM) is located at Γ -valley, whereas the energy of K-valley is close to Γ -valley and contributes to the VBM. The contours around Γ -valley are isotropic and circular, whereas K-valley demonstrates anisotropic behavior and is close to triangular.

The band structures along the high symmetry points for four compounds are depicted in Fig. 3. The CBM is located at K-valley in all compounds, whereas in α_2 -structures, the energy of M-point is close to CBM, especially for α_2 - WSi_2N_4 . On the other hand, the VBM is placed at Γ -point and the energy of K-point is close to VBM. The corresponding projected density of states (PDOS) are plotted beside the band structures. PDOS demonstrates that both conduction and valence bands are highly comprised of the d-orbitals from Mo or W elements. In addition, the p-orbitals of N atoms also contribute to the conduction and valence bands. The p-orbitals of Si atoms have an influence on the higher energies in the conduction band and do not contribute to the CBM and VBM.

The electrical properties of these four monolayers are listed in Table II. The bandgap of α_1 -configuration of MoSi_2N_4 is 1.748 eV that is in good agreement with previous results [18], [21]. However, α_2 one has a higher bandgap as 1.954 eV that is approximately 0.2 eV higher than α_1 . The bandgap of α_1 - WSi_2N_4 also is 2.129 eV that is close to the previous reported values [18], [21]. The bandgap increases to 2.41 eV for α_2 -structures that is 0.3 eV larger than its α_1 -configuration. The results prove that α_2 constructions demonstrate a higher bandgap. As one can see, the CBM and VBM are located at K- and Γ -valleys, respectively. The effective masses of important valleys in the conduction and valence bands are reported in Table II. In the valence band, the effective masses

of Γ -valley in different directions are approximately the same, whereas K-valley demonstrates various effective masses along different directions. Previously, we have observed in Fig. 2 isotropic and anisotropic contours around Γ - and K-point, respectively. Γ -valley demonstrates a higher effective mass with respect to K-valley that is compatible with the corresponding band structure. In addition, α_2 -structures show larger effective masses along with its higher bandgap. For example, the effective mass of α_1 - MoSi_2N_4 in the Γ -valley is 1.31 m_0 , while increases to 1.6 m_0 for α_2 one. Although α_2 -structure contains the higher effective mass, this configuration shows lower anisotropy at K-valley. For instance, the effective masses of α_1 - WSi_2N_4 are 0.728 and 0.569 m_0 and for α_2 - WSi_2N_4 are 0.797 and 0.727 m_0 along $K \rightarrow M$ and $K \rightarrow \Gamma$ paths of valence band, respectively. The difference between the effective masses along different paths for α_1 - and α_2 -structures are 0.16 and 0.07 m_0 that proves α_2 -structure demonstrates lower anisotropy at K-valley.

The biaxial in-plane strain has been known as a powerful tool to modify the electrical and electronic properties of 2D materials [31], [32]. The biaxial strain has been applied to four compounds and their electronic properties are explored. First of all, the band gaps of these four materials with respect to the strain are presented in Fig. 4(a). The band gaps of all compounds show a maximum at a compressive strain between -2% and -4%. Then, the band gaps decrease under compressive and tensile strains. The strain value is swept from -15 to 15%. While the bandgap of α_1 - MoSi_2N_4 closes under a tensile strain of 15%, the bandgap is higher than 1eV at a compressive strain of 15%. Under compressive strains lower than -5%, the band gaps of all compounds are approximately the same, whereas the band gaps exhibit different values on the other

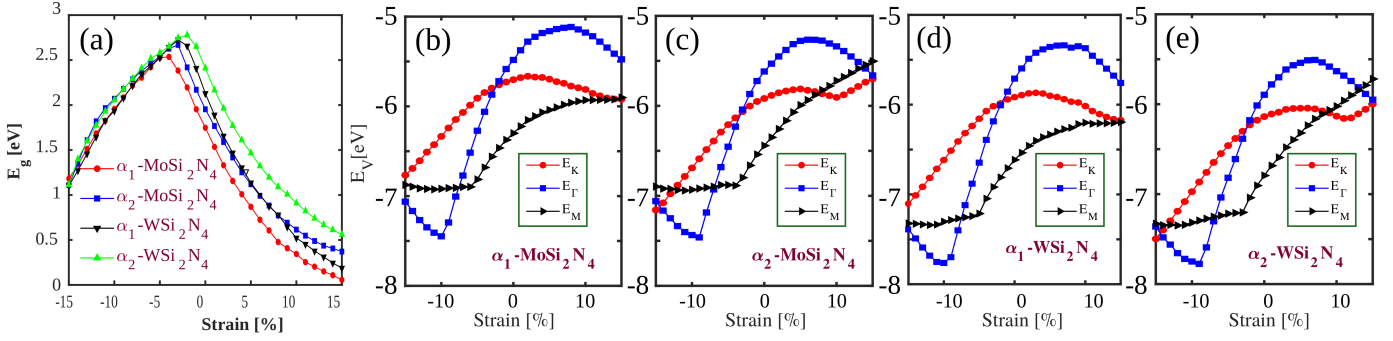


Fig. 4. (a) The band gap variations as a function of in-plane biaxial strain for four compounds. (b-e) The energies of the valence band valleys as a function of the biaxial strain for Γ -valley (E_V), K-valley (E_K), and M-valley (E_M).

side of the maximum point. The band gaps also decrease more rapidly at low tensile strains and the α_1 -structures show the lowest band gaps in large tensile strains.

It has been reported in the experimental works that monolayer MoSi₂N₄ demonstrates a p-type characteristic [21]. In this regard, the valence band (hole) properties are investigated in the following. For clarifying the behavior of the valleys, the energies of the effective valleys in the valence bands with respect to strain are plotted in Fig. 4(b-e). Three valleys (Γ , K and M) participate at the valence band. The VBM is located at Γ -valley in the tensile strain, whereas K- and M-valleys also contribute to the VBM of α_2 -structures at the large tensile strains. At these strains, the M-valley is dominant and two other valleys also contribute VBM. Γ - and K-valleys on valence band possess the close energy at small compressive strains while the K-valley is dominant at compressive strains. Similar to the large tensile strains, three valleys contribute to the VBM of α_2 -structures at the large compressive strains.

The hole effective mass has been explored under various strains. The effective masses of these two valleys versus strain are reported in Fig. 5. Two K- and Γ -valleys, contribute to the VBM in the most range of strain. The K-valley exhibits the lowest effective mass at compressive strains and one can find from Fig. 4 that the VBM is located at K-valley in this strain range. The values of the K-valley effective masses increase as the strain changes from compressive to the tensile regime. In addition, in α_1 structures two different paths at K-valley demonstrate different effective masses, whereas these two paths possess the same value for α_2 ones. The difference of two effective masses in α_1 structures increases with a rise in the strain and K-valley shows more anisotropy for tensile strains. At the same time, the effective mass of Γ -valley decreases with the strain and becomes the lowest effective mass at tensile strains. At the tensile regime, the VBM is located at Γ -valley. The Γ -valley demonstrates isotropic effective mass for a wide range of strain and only shows anisotropic effective mass at large compressive strain, where it does not contribute to the VBM. The effective masses for both MoSi₂N₄ and WSi₂N₄ behave similarly. However, WSi₂N₄ demonstrates a little lower effective mass.

The electronic properties of the DGFET with strained MoSi₂N₄ and WSi₂N₄ as the channel material is investigated through the top of the barrier model [13], [33]. These materials

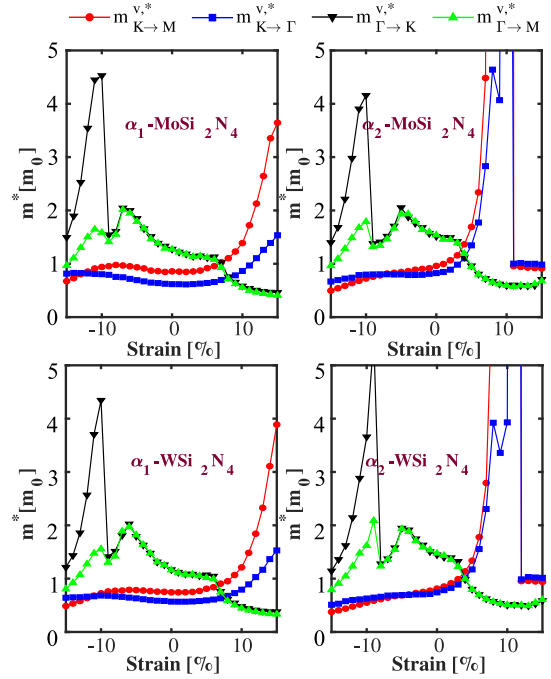


Fig. 5. The hole effective masses as a function of strain at two effective valleys (K and Γ). The effective masses of Γ -valley along Γ to K ($m_{\Gamma \rightarrow K}^{v,*}$) and Γ to M ($m_{\Gamma \rightarrow M}^{v,*}$) and effective masses of K-valley along K to Γ ($m_{K \rightarrow \Gamma}^{v,*}$) and K to M ($m_{K \rightarrow M}^{v,*}$) are plotted.

indicate p-type behavior at experiment results and here, a p-type FET (PMOS) is also investigated. Drain current (I_{DS}) versus drain-source voltage (V_{DS}) is drawn in Fig. 6. I_{DS} increases at small drain voltages and it saturates around $V_{DS} = 0.1V$. Then, I_{DS} continues to increase with a small slope. Drain current is also investigated under different values of strains. The equilibrium condition and large compressive strains demonstrate the lowest and highest current in the α_1 -structures, respectively. On the other hand, the large tensile and the compressive strain demonstrate the lowest and highest current for the α_2 -structures, respectively. The equal energy of K- and Γ -valleys at equilibrium state for all structures results in the high effective mass and small current.

The drain current as a function of gate voltage for different strain values is shown in Fig. 7. For better understanding, the drain current is studied at both linear and logarithmic

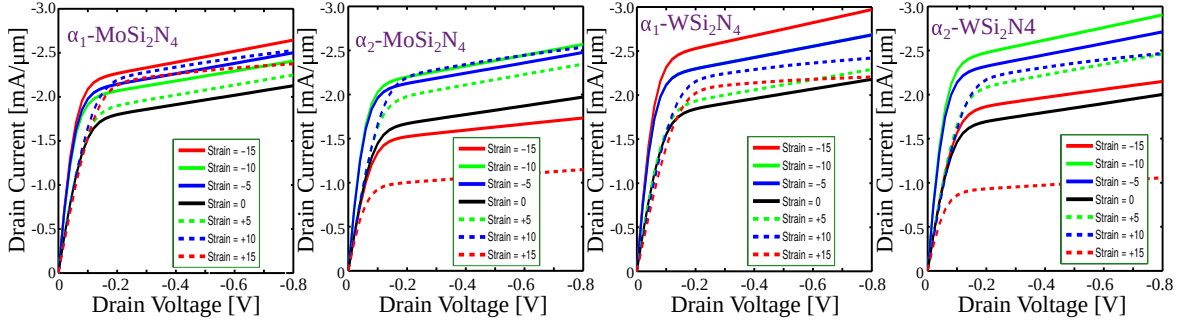


Fig. 6. The current-voltage characteristic of DGFET with MoSi_2N_4 and WSi_2N_4 as the channel material under biaxial strain.

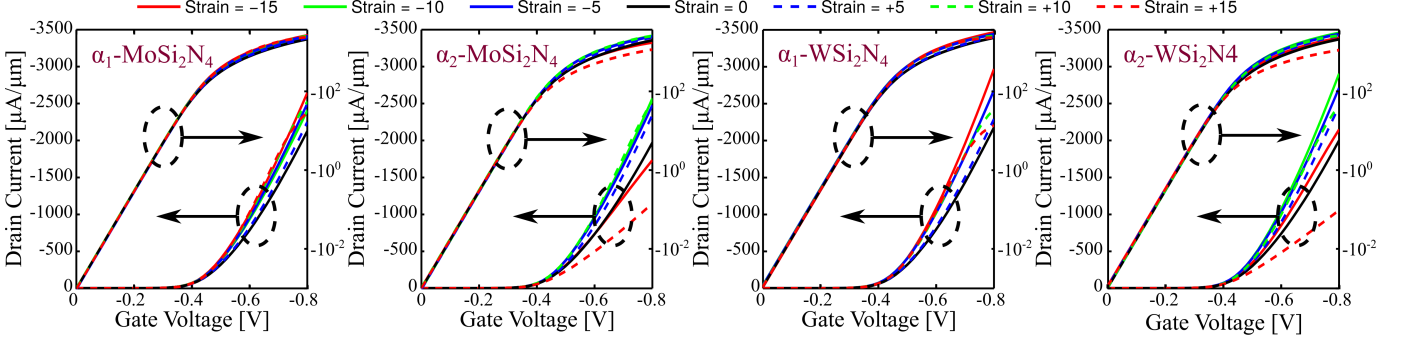


Fig. 7. The drain current versus gate voltage of studied DGFET under different values of strains in two linear and logarithmic scales.

scales. The linear scale clarifies the ON-current performance and follows the $I_{DS}-V_{DS}$ behavior. The ON-current, OFF-current and I_{ON}/I_{OFF} ratio for four compounds are obtained in the range of $2000-2200\mu\text{A}/\mu\text{m}$, $10^{-3}\mu\text{A}/\mu\text{m}$, and $2.0-2.2\times 10^6$, respectively. These values are comparable with FET based on the other monolayers [34]–[38]. The steep rising of the current in the sub-threshold region is obvious from the logarithmic scale and results in a small sub-threshold swing (SS). The four compounds indicate similar SS in the range of 96-98 mV/dec. Indeed, the SS is controlled by the FET structure more than channel material.

One of the most important parameters of the FETs is I_{ON}/I_{OFF} ratio. The I_{ON}/I_{OFF} ratio is over 10^6 for nowadays technologies. The obtained I_{ON}/I_{OFF} ratio versus biaxial strain for all four compounds are plotted in Fig. 8. All curves demonstrate a minimum at small compressive strains close to the equilibrium condition. At these strains, both K- and Γ -valley possess the same energy that results in a high effective mass. This high effective mass leads to a small ON-current and consequently small I_{ON}/I_{OFF} ratio. In addition, the α_2 -structures display other minimums at -15 and +15% strains. In these strains, three valleys (Γ , K and M) have the same energy that results in a high effective mass and low ON-current. However, K- and Γ -valley are dominant at these strain values. The I_{ON}/I_{OFF} ratio follows the effective mass behavior out of these minimums. Γ -valley is dominant over tensile strains and controls the current. The reduction of the effective mass of Γ -valley at tensile strains increases the ON-current and I_{ON}/I_{OFF} ratio. One can observe a jump in the I_{ON}/I_{OFF} ratio for moderate tensile strains. Such a jumping has been seen in the effective mass of Γ -valley at

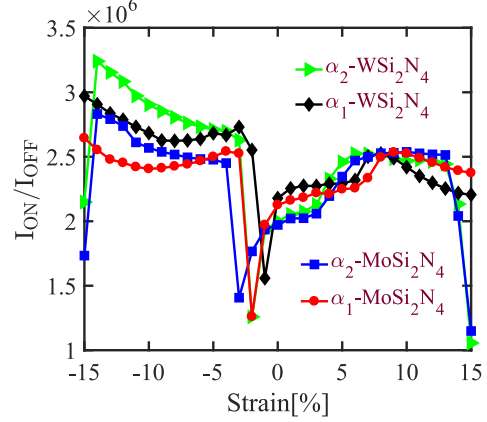


Fig. 8. The I_{ON}/I_{OFF} ratio as a function of strain for DGFETs with studied compounds as the channel material.

tensile strains. On the other hand, the VBM is determined by K-valley at compressive strains. The effective mass of K-valley increases for small compressive strain and decreases for larger compressive strains. I_{ON}/I_{OFF} ratio also decreases for small compressive strains but increases for larger compressive strains.

IV. CONCLUSION

The electronic properties and performance of DGFETs based on two different configurations of monolayer MSi_2N_4 ($M = \text{Mo}, \text{W}$) under biaxial strain are investigated. These materials exhibit indirect bandgap with CBM and VBM at K- and Γ -valleys, respectively. The α_2 -configurations demonstrate

a higher bandgap along with larger effective masses. The Γ -valley demonstrates equal effective masses along different directions, whereas K-valley has anisotropic effective masses. The band gaps and effective masses can be tuned by in-plane biaxial strain. All compounds show a maximum value of bandgap at compressive strains between -2% and -4%. Afterward, the bandgap decreases for both compressive and tensile strains. Finally, the current-voltage characteristic of p-type FET with MSi_2N_4 as the channel has been explored. I_{DS} increases at small values of V_{DS} until its saturation around $V_{DS} = 0.1\text{V}$. The I_{ON}/I_{OFF} ratio is larger than 10^6 and sub-threshold swing is obtained in the range of 96-98 mV/dec. Furthermore, bi-axial strain can effectively modulate the current-voltage characteristic of DGFETS. The I_{ON}/I_{OFF} ratio with respect to strain demonstrates a minimum at small compressive strains close to equilibrium condition for all materials. Γ -valley is dominant over tensile strains and controls the current. The reduction of the effective mass of Γ -valley at tensile strains increases the ON-current and I_{ON}/I_{OFF} ratio.

REFERENCES

- [1] K. S. Novoselov, A. K. Geim, S. Morozov, D. Jiang, Y. Zhang, S. Dubonos, I. Grigorieva, and A. Firsov, "Electric field effect in atomically thin carbon films," *Science*, vol. 306, no. 5696, pp. 666–669, 2004.
- [2] Y.-M. Lin, C. Dimitrakopoulos, K. A. Jenkins, D. B. Farmer, H.-Y. Chiu, A. Grill, and P. Avouris, "100-GHz transistors from wafer-scale epitaxial graphene," *Science*, vol. 327, no. 5966, pp. 662–662, 2010.
- [3] H. Wang, D. Nezich, J. Kong, and T. Palacios, "Graphene frequency multipliers," *IEEE Electron Device Lett.*, vol. 30, no. 5, pp. 547–549, 2009.
- [4] C. R. Dean, A. F. Young, I. Meric, C. Lee, L. Wang, S. Sorgenfrei, K. Watanabe, T. Taniguchi, P. Kim, K. L. Shepard *et al.*, "Boron nitride substrates for high-quality graphene electronics," *Nat. Nanotechnol.*, vol. 5, no. 10, pp. 722–726, 2010.
- [5] Y. Zhang, T.-T. Tang, C. Girit, Z. Hao, M. C. Martin, A. Zettl, M. F. Crommie, Y. R. Shen, and F. Wang, "Direct observation of a widely tunable bandgap in bilayer graphene," *Nature*, vol. 459, no. 7248, pp. 820–823, 2009.
- [6] P. Gava, M. Lazzeri, A. M. Saitta, and F. Mauri, "Ab initio study of gap opening and screening effects in gated bilayer graphene," *Phys. Rev. B*, vol. 79, no. 16, p. 165431, 2009.
- [7] Y.-W. Son, M. L. Cohen, and S. G. Louie, "Energy gaps in graphene nanoribbons," *Phys. Rev. Lett.*, vol. 97, no. 21, p. 216803, 2006.
- [8] G. Giovannetti, P. A. Khomyakov, G. Brocks, P. J. Kelly, and J. Van Den Brink, "Substrate-induced band gap in graphene on hexagonal boron nitride: Ab initio density functional calculations," *Phys. Rev. B*, vol. 76, no. 7, p. 073103, 2007.
- [9] Q. Fu, J. Han, X. Wang, P. Xu, T. Yao, J. Zhong, W. Zhong, S. Liu, T. Gao, Z. Zhang *et al.*, "2D transition metal dichalcogenides: Design, modulation, and challenges in electrocatalysis," *Advanced Materials*, vol. 33, no. 6, p. 1907818, 2021.
- [10] M. Hosseini, M. Elahi, M. Pourfath, and D. Esseni, "Strain-induced modulation of electron mobility in single-layer transition metal dichalcogenides MX_2 (M= Mo, W; X= S, Se)," *IEEE Trans. Electron Devices*, vol. 62, no. 10, pp. 3192–3198, 2015.
- [11] M. Hosseini, H. Karami, and Z. Sohrabi, "Investigation of layer number effects on the electrical properties of strained multi-layer mos 2," *J. Comput. Electron.*, vol. 18, no. 4, pp. 1236–1242, 2019.
- [12] Y. Guo and J. Robertson, "Band structure, band offsets, substitutional doping, and schottky barriers of bulk and monolayer InSe ," *Phys. Rev. Mater.*, vol. 1, no. 4, p. 044004, 2017.
- [13] S. B. Touski, M. Ariapour, and M. Hosseini, "Electrical and electronic properties of strained mono-layer InTe ," *Physica E*, vol. 118, p. 113875, 2020.
- [14] M. Elahi, K. Khaliji, S. M. Tabatabaei, M. Pourfath, and R. Asgari, "Modulation of electronic and mechanical properties of phosphorene through strain," *Phys. Rev. B*, vol. 91, no. 11, p. 115412, 2015.
- [15] S. K. Ghosh and D. Mandal, "Piezoelectricity of 2D materials and its applications toward mechanical energy harvesting," in *2D Nanomaterials for Energy Applications*. Elsevier, 2020, pp. 1–38.
- [16] M. Springolo, M. Royo, and M. Stengel, "Flexoelectricity in two-dimensional materials," *arXiv preprint arXiv:2010.08470*, 2020.
- [17] Q. Wang, L. Cao, S.-J. Liang, W. Wu, G. Wang, C. H. Lee, W. L. Ong, H. Y. Yang, L. K. Ang, S. A. Yang *et al.*, "Designing efficient metal contacts to two-dimensional semiconductors MoSi_2N_4 and WSi_2N_4 monolayers," *arXiv preprint arXiv:2012.07465*, 2020.
- [18] L. Wang, Y. Shi, M. Liu, A. Zhang, Y. Hong, R. Li, Q. Gao, M. Chen, W. Ren, H. Cheng, Y. Li, and X. Chen, "Intercalated architecture of ma_2z_4 family layered van der waals materials with emerging topological, magnetic and superconducting properties," *Nat. Commun.*, vol. 12, no. 1, 2021.
- [19] H. Zhong, W. Xiong, P. Lv, J. Yu, and S. Yuan, "Strain-induced semiconductor to metal transition in MA_2Z_4 bilayers (M= Ti, Cr, Mo; A= Si; Z= N, P)," *Phys. Rev. B*, vol. 103, no. 8, p. 085124, 2021.
- [20] B. Mortazavi, B. Javvaji, F. Shojaei, T. Rabczuk, A. V. Shapeev, and X. Zhuang, "Exceptional piezoelectricity, high thermal conductivity and stiffness and promising photocatalysis in two-dimensional MoSi_2N_4 family confirmed by first-principles," *Nano Energy*, vol. 82, p. 105716, 2021.
- [21] Y.-L. Hong, Z. Liu, L. Wang, T. Zhou, W. Ma, C. Xu, S. Feng, L. Chen, M.-L. Chen, D.-M. Sun *et al.*, "Chemical vapor deposition of layered two-dimensional MoSi_2N_4 materials," *Science*, vol. 369, no. 6504, pp. 670–674, 2020.
- [22] Y. Cai, G. Zhang, and Y.-W. Zhang, "Polarity-reversed robust carrier mobility in monolayer mos_2 nanoribbons," *J. Am. Chem. Soc.*, vol. 136, no. 17, pp. 6269–6275, 2014.
- [23] S. B. Touski and N. Ghobadi, "Vertical strain-induced modification of the electrical and spin properties of monolayer MoSi_2X_4 (X= N, P, As and Sb)," *arXiv preprint arXiv:2106.07081*, 2021.
- [24] C. Yang, Z. Song, X. Sun, and J. Lu, "Valley pseudospin in monolayer MoSi_2N_4 and MoSi_2As_4 ," *Phys. Rev. B*, vol. 103, no. 3, p. 035308, 2021.
- [25] Q. Li, W. Zhou, X. Wan, and J. Zhou, "Strain effects on monolayer $\text{mosi}2\text{n}4$: ideal strength and failure mechanism," *Physica E*, vol. 131, p. 114753, 2021.
- [26] A. Rahman, J. Guo, S. Datta, and M. S. Lundstrom, "Theory of ballistic nanotransistors," *IEEE Trans. Electron Devices*, vol. 50, no. 9, pp. 1853–1864, 2003.
- [27] M. Hosseini and H. Karami, "Strain effects on the dc performance of single-layer tmd-based double-gate field-effect transistors," *J. Comput. Electron.*, vol. 17, no. 4, pp. 1603–1607, 2018.
- [28] J. M. Soler, E. Artacho, J. D. Gale, A. García, J. Junquera, P. Ordejón, and D. Sánchez-Portal, "The siesta method for ab initio order-n materials simulation," *J. Phys.:Condensed Matter*, vol. 14, no. 11, p. 2745, 2002.
- [29] J. P. Perdew and A. Zunger, "Self-interaction correction to density-functional approximations for many-electron systems," *Phys. Rev. B*, vol. 23, no. 10, p. 5048, 1981.
- [30] A. Kokalj, "Computer graphics and graphical user interfaces as tools in simulations of matter at the atomic scale," *Comput. Mater. Sci.*, vol. 28, no. 2, pp. 155–168, 2003.
- [31] S. B. Touski and N. Ghobadi, "Interplay between stacking order and in-plane strain on the electrical properties of bilayer antimonene," *Physica E*, p. 114407, 2020.
- [32] S. Babaee Touski and N. Ghobadi, "Structural, electrical, and rashba properties of monolayer janus $\text{si}2\text{xy}$ (x, y= p, as, sb, and bi)," *Phys. Rev. B*, vol. 103, no. 16, p. 165404, 2021.
- [33] H. Manouchehr and B. T. Shoeib, "Investigation of double-gate ferroelectric FET based on single-layer MoS_2 with consideration of contact resistance," *J. Electron. Mater.*, vol. 49, no. 7, pp. 4085–4090, 2020.
- [34] A. Sengupta, R. K. Ghosh, and S. Mahapatra, "Performance analysis of strained monolayer mos_2 mosfet," *IEEE Trans. Electron Devices*, vol. 60, no. 9, pp. 2782–2787, 2013.
- [35] D. Yin, G. Han, and Y. Yoon, "Scaling limit of bilayer phosphorene fets," *IEEE Electron Device Lett.*, vol. 36, no. 9, pp. 978–980, 2015.
- [36] A. Mukhopadhyay, S. Kanungo, and H. Rahaman, "The effect of the stacking arrangement on the device behavior of bilayer mos 2 fets," *J. Comput. Electron.*, vol. 20, no. 1, pp. 161–168, 2021.
- [37] E. G. Marin, D. Marian, G. Iannaccone, and G. Fiori, "First-principles simulations of fets based on two-dimensional inse," *IEEE Electron Device Lett.*, vol. 39, no. 4, pp. 626–629, 2018.
- [38] Y. Ouyang, Y. Yoon, and J. Guo, "Electron device lett," *IEEE*, vol. 54, p. 2223, 2007.